International Forum on Aeroelasticity and Structural Dynamics
IFASD 2024
17-21 June 2024, The Hague, The Netherlands

TRANSONIC AEROELASTIC LIMIT CYCLES AND THEIR DEPENDENCE ON FREESTREAM CONDITIONS

Nicholas F. Giannelis[1]

[1]The University of New South Wales, Canberra,
School of Engineering and Technology, Campbell, ACT, 2612, Australia
n.giannelis@unsw.edu.au

Keywords: Transonic Buffet; Transonic Aeroelasticity; Limit Cycle Oscillations; Computational Fluid Dynamics.

Abstract: In this paper, Unsteady Reynolds-Averaged Navier-Stokes (URANS) flow simulations are coupled to a single-degree-of-freedom rigid body structural solver to study the dependence of the transonic aeroelastic response of the OAT15A to variations in freestream conditions. The aeroelastic computations are validated against elastically-suspended profile wind tunnel experiments, with excellent correlation in the unsteady loads and surface pressure magnitude and phase. Mach number and angle of attack sweeps are performed for three distinct structural configurations, with the pitch eigenfrequency below, marginally above and well-above the buffet frequency. The results find a rich spectrum of nonlinear dynamic behaviour, including mode-switching, asymmetric LCOs, and Hopf and jump bifurcations. Of significance is the emergence of nontypical LCOs for the structural composition in which frequency lock-in was observed. The origins of nontypical limit cycles, which grow and then reduce in amplitude with increases in Mach number, have been debated in literature and the findings of the present study indicate a potential connection between this transonic aeroelastic phenomenon and buffet lock-in.

1 INTRODUCTION

At conditions near the bounds of conventional flight envelopes, aircraft may encounter large-scale flow unsteadiness, with the potential to incite adverse aeroelastic behaviours. For turbulent Reynolds numbers in the transonic regime, this flow unsteadiness may manifest as transonic buffet; aerodynamic limit cycle oscillations (LCOs) involving self-sustained shock motions at reduced frequencies typically of comparable order to the low-frequency structural modes. The subsequent aeroelastic response of an air vehicle subject to transonic buffet is undesirable and poses both controllability and fatigue-life issues for the structure.

To confidently expand the flight envelope of next-generation air vehicles, a comprehensive understanding of these edge-of-the-envelope flight phenomena is required. Significant research efforts have been devoted to the study of transonic buffet over rigid profiles. For instance, Giannelis et. al [1] found a highly nonlinear dependence of the unsteady load fluctuation magnitude and frequency on both angle of attack and Mach number. Many studies have also considered elastic wing-sections subject to buffet at a nominal freestream condition with varying structural properties. Raveh & Dowell [2] is one such example, where an increase in the structural pitch natural frequency beyond the buffet frequency was found to incite synchronisation (lock-in)

behaviour in the aeroelastic response. Nonetheless, relatively few studies have sought to investigate the sensitivity of the aeroelastic buffet response to changes in freestream conditions; that is the goal of the present work.

This study applies Unsteady Reynolds-Averaged Navier-Stokes (URANS) flow simulations coupled to a single-degree-of-freedom rigid body structural solver to investigate the relationship between freestream flow conditions and the transonic aeroelastic response of the OAT15A aerofoil profile. The paper proceeds as follows: Section 2 outlines the methodology employed throughout the study, including a brief description of the test case, the numerics of the fluid domain modelling and means by which aeroelastic coupling has been implemented. Section 3 then provides necessary preliminaries for interpretation of the key results, including the variation in rigid-profile buffet response over a range of freestream conditions, validation of the aeroelastic computations and baseline aeroelastic responses at a nominal flight condition. The key results are presented in Section 4, which analyses the influence of flight condition on transonic aeroelastic limit cycles from a nonlinear dynamics perspective. The paper then concludes in Section 5 with a summary of key findings.

2 METHODOLOGY

2.1 Test case

Owing to the wealth of validation data available, the OAT15A supercritical profile is selected as the test case in this study. This aerofoil has been subject to an extensive experimental buffet campaign in the S3Ch Continuous research Tunnel at ONERA Chalais-Meudon. Jacquin et al. [3] has detailed results for a rigid profile subject to Mach number and angle of attack sweeps in the vicinity of buffet onset, where steady and unsteady pressure, surface stream oil flow, Laser Doppler Velocimetry and Schlieren imaging measurements have been collected and enables the validation of computational buffet simulations. The nominal freestream condition of Reynolds number $Re \approx 3 \times 10^6$, Mach number $M = 0.73$, and angle of attack $\alpha = 3.5^\circ$ represents a developed buffet state. Nonetheless, the experiments of Jacquin et al. [3] found a dependence of both pressure fluctuation amplitude and frequency on Mach number and angle of attack. In this study, the influence of these changes in freestream conditions on the aeroelastic response of an elastically-suspended OAT15A profile is considered numerically.

2.2 Flow modelling

Simulations in this study have been performed using the cell-centred, finite-volume commercial Computational Fluid Dynamics code ANSYS Fluent R18.2 [4]. The two-dimensional density-based implicit solver is employed to formulate the coupled set of continuity, momentum and energy equations. Euler fluxes are computed through an upwind Roe flux difference splitting scheme, with extrapolation of convective variables performed using the blended central-difference/second-order upwind Monotone Upstream-Centred Scheme for Conservation Laws (MUSCL) scheme. Diffusive fluxes are resolved using a second-order central difference scheme, with gradient reconstruction of all terms realised by the cell-based least-squares method and solved by Gram-Schmidt decomposition of the cell coefficient matrix. Menter's k-ω Shear-Stress Transport (SST) model [5] is employed for turbulent closure of the Navier-Stokes equations, with previous investigations by the authors demonstrating excellent correlation in unsteady loads between computation and experiment applying this modelling approach [1, 6]. A second-order backward Euler dual time stepping scheme is used for temporal discretisation, with pseudo-time convergence achieved when the relative change in integral aerodynamic coefficients between successive subiterations falls below 10^{-7}. All computations are performed

using a CH-type quadrilateral grid of approximately 48000 cells and with a nondimensional time-step of $\Delta\tau = 0.01$, with this workflow again verified by the author in earlier studies [1,6].

2.3 Aeroelastic modelling

The aeroelastic system in the present study is modelled primarily as a Single Degree-of-Freedom (SDOF) linear spring-mass-damper constrained to motion in the pitch degree-of-freedom. Fluent's Six-DOF Rigid body solver [4] is employed to integrate the structural equations of motion, marching forward in time with a second-order accurate backward Euler scheme. The equation of motion governing the aeroelastic system is given by:

$$I_\theta(\ddot{\theta} + 2\zeta_\theta\omega_\theta\dot{\theta} + \omega_\theta^2\theta) = M_{cg} \tag{1}$$

where θ, $\dot{\theta}$ and $\ddot{\theta}$ are the pitch displacement, velocity and acceleration, respectively, ω_θ is the pitch natural angular frequency, ζ_θ is the pitch damping ratio and M_{cg} is the pitching-moment about the centre of gravity (CG), nominally at 40% chord. The elastic axis and centre of gravity are enforced to be coincident such that all moments in Equation 1 are taken about the centre of gravity. The pitch moment of inertia I_θ is computed by:

$$I_\theta = \mu\pi\rho b^3 r_\theta^2 \tag{2}$$

where ρ is the freestream density, b is the aerofoil semi-chord and $r_\theta^2 = 0.75$ is the radius of gyration, which is held constant across all simulations. The parameter μ is the sectional mass ratio, given by:

$$\mu = \frac{m}{\pi\rho b^2} \tag{3}$$

where m is the section mass. For validation of the aeroelastic solver, two degree-of-freedom uncoupled pitch and heave motion is considered. In this instance, the SDOF heave motion is dictated by:

$$m(\ddot{h} + 2\zeta_h\omega_h\dot{h} + \omega_h^2 h) = L \tag{4}$$

where h, $\dot{h}$ and $\ddot{h}$ are heave displacement, velocity and acceleration respectively, ω_h is the heave natural angular frequency, ζ_h is the pitch damping ratio and L is the vertical force on the aerofoil section.

For the aeroelastic simulations that follow, a nominal structural configuration of $\mu = 100$ and $\zeta = 1\%$ is chosen. These cases are initialised with the steady-state aerodynamic limit cycle solution of the rigid aerofoil. Further, to mitigate the influence of static aeroelastic deflections, the torsional and/or linear springs are pre-stressed to negate the pitching-moment and/or lift in the pitch and heave simulations, respectively. As the base flow is inherently unsteady, these offsets are taken as the mean of the fluctuating pitching-moment and vertical force computed for the rigid profile.

3 NECESSARY PRELIMINARIES

3.1 Rigid buffet response

The influence of changes in freestream conditions to the unsteady aerodynamic response of a wing section subject to transonic buffet is well documented in the literature [1, 7]. Here, the key relationships are reiterated as preliminary considerations for the analysis of the aeroelastic responses. Figure 1 provides a mapping of the buffet envelope for the OAT15A profile across a range of Mach numbers and angles of attack at $Re = 3 \times 10^6$, where the onset and offset

states are defined by conditions where unsteady lift fluctuations $\Delta C_L < 0.05$. Markers indicate conditions at which simulations have been performed, with interpolation contours provided by a Radial Basis Function (RBF) surrogate model constructed with a Gaussian basis, as outlined by Forrester & Keane [8].

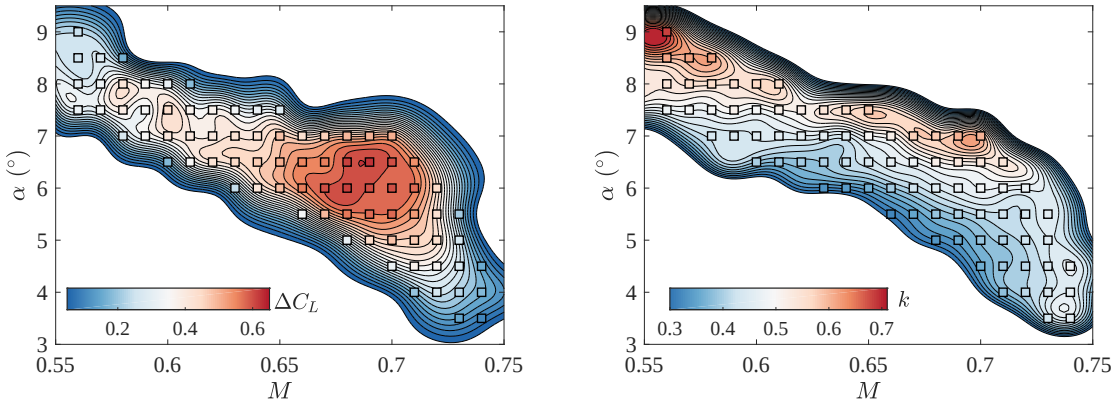

(a) Amplitude

(b) Frequency

Figure 1: Buffet amplitude and frequency variations in $M - \alpha$ space for the OAT15A profile.

The buffet amplitude contours of Figure 1(a) define the variation in peak-to-peak lift coefficient at varying freestream conditions, demonstrating the abrupt onset and offset of large-scale flow unsteadiness within the buffet envelope. It is stressed that comparable behaviour also observed in both the pitching moment and drag coefficients. For a given Mach number, the buffet amplitude variation is concave with increasing incidence; peaking near the centre of the envelope and then diminishing towards offset. Comparable behaviour is also observed with an increase in Mach number for $\alpha < 7°$. At high incidence, the relationship between amplitude and Mach number is more complex. Figure 1(a) shows a trimodal character, with three distinct peaks in maximum lift differential observed as Mach number varies. Such behaviour results from the changing nature of the shock dynamics, as described by Giannelis et al. [6].

The buffet frequency contours provided in Figure 1(b) indicate the variation in the dominant reduced frequency of the lift oscillations, as computed via Fast Fourier Transform of the lift signals, across the buffet envelope. Relative to the buffet amplitude contours of Figure 1(a), the change in dominant reduced frequency is somewhat more predictable; increasing monotonically with both angle of attack and Mach number. The magnitude of this variation in reduced frequency throughout the instability bounds is significant, with a maximum $\Delta k \approx 0.4$ observed across the considered flight conditions. The implications of this frequency shift for an aeroelastic system subject to unsteady aerodynamic excitation have been stressed by several authors [9–12]. The interaction between an oscillating shock wave and a structural mode may yield excitation of large amplitude structural limit cycles, particularly if the excitation frequency is comparable to a structural natural frequency, increasing the likelihood of modal synchronisation. Figure 1(b) indicates that such an interaction may be flight condition dependent. Additionally, variation in the freestream conditions may incite higher-order aerodynamic modes. To illustrate this point, Figure 2 shows the lift time and frequency responses for three distinct conditions within the buffet envelope. At lower Mach numbers and higher angles of attack, pronounced superharmonics are evident in the aerodynamic response, indicating a likely change in the nature of the aeroelastic response with a shift in modal excitation. The relationship between these interactions is explored further in Section 4.

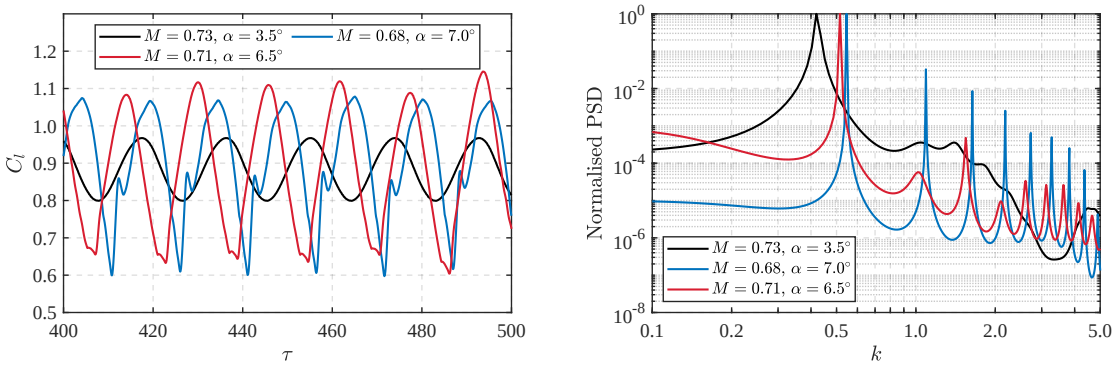

(a) Time history

(b) PSDs

Figure 2: Lift coefficient time and frequency responses at varying freestream conditions.

3.2 Validation of the aeroelastic simulations

Section 2.2 and prior studies [1] detail validation efforts of the numerical workflow employed in the current work for rigid buffet simulations. To gain confidence in the methodology employed in the aeroelastic simulations, the dynamic response of the OAT15A under sinusoidal gust excitation is compared to additional dynamic experiments on the profile conducted by ONERA [13–16].

Huvelin et. al. [16] detail an experimental and numerical test campaign dedicated to transonic gust load prediction and control. Under this project, the authors present the development of an experimental gust generator comprised of two aerofoils situated upstream of the wind tunnel test section, in addition to a pitch-heave aeroelastic rig to assess the dynamic response of a profile subject gust excitation. While the experimental programme spanned a number of freestream conditions, gust input definitions and structural configurations, the data at $M = 0.73$, $\alpha = 2°$ and $Re = 3.3 \times 10^6$ are employed in this study. This condition is in the vicinity of shock buffet onset for the OAT15A, and the unsteady motions incited by the gust excitation offer a reasonable analogue to the autonomous shock motions experienced within the buffet envelope.

The gust excitation is incorporated in the simulations via a source term in the y-momentum equations, in a manner similar to Goluven et. al. [17] and differing from prior work [18] in which the excitation loads were directly imposed on the structural system. As Huvelin et. al. [16] have shown that the developed gust generator does not significantly perturb the streamwise flow through the centre of the test section, an x-momentum forcing is not included. Alternate implementations, such as imposing a time-dependent boundary condition or employing the field-velocity approach [19, 20] were also considered. Simulations including a time-dependent boundary condition resulted in substantial diffusion of the gust field as the flow convected towards the profile, rendering the method ineffective. An efficient implementation of the field-velocity approach, which imposes the gust by imparting a grid velocity within the computational domain [21], was also problematic considering the restricted access to source code that stems from the use of a commercial software package. Nonetheless, the y-momentum forcing method employed herein is shown below to effectively reproduce an equivalent gust response to that of Huvelin et. al. [16].

A rigid validation case is first considered corresponding to a sinusoidal gust field with gust amplitude of 0.5% of the freestream velocity and a frequency of 30 Hz. The gust velocity is converted to an equivalent momentum, which is imposed within a region of the computational

domain centred two chord lengths upstream of the profile and spanning one chord length in either direction. Figure 3 shows the development of the gust field with time $\tilde{\tau}_g$ (normalised by the gust period) at three locations upstream of the profile. The normalised gust velocity $\tilde{w}_g$ represents the additional vertical velocity imposed by the gust field above the freestream value, normalised by the freestream velocity. Figure 3(a) shows a sinusoidal velocity fluctuation in time within the gust generator region of the domain. As the gust convects downstream it interacts with the velocity field of the profile, as shown in Figures 3(b) and 3(c).

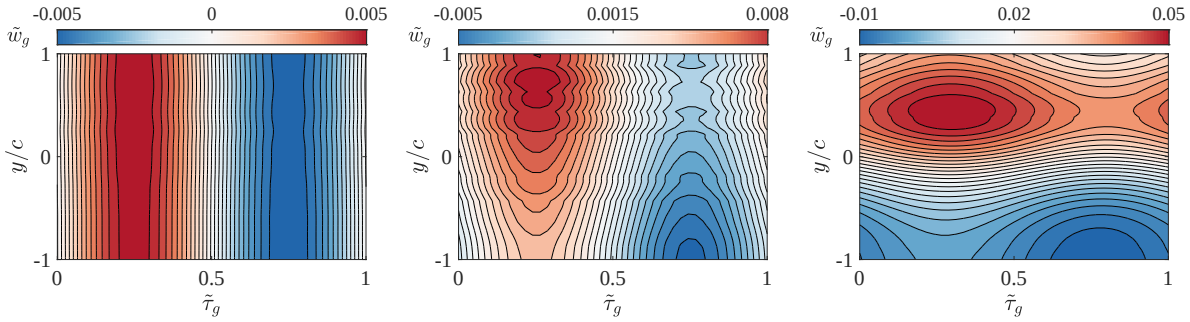

(a) $x/c = -1.5$ (b) $x/c = -1.0$ (c) $x/c = -0.5$

Figure 3: Development of normalised vertical velocity field due to gust during convection towards the profile.

Figure 4 then shows a comparison between the experimental and computed lift coefficient time history and mean surface pressure coefficient. The simulations marginally overestimate the mean lift and predict a mean shock location slightly downstream. Some deviation is also evident in the bump like character in the post-shock pressure recovery. Such behaviour was also seen in the computations performed by Huvelin et. al. [16]. In the original work, the authors saw improvements in the pressure distribution by accurately modelling the wind-tunnel, along with the upstream oscillating aerofoils that generate the gust field. Further, an optimisation routine was employed to determine appropriate wind-tunnel correction factors for their freestream calculations. Considering the assumptions made in the present work, the experimental results are generally well-reproduced.

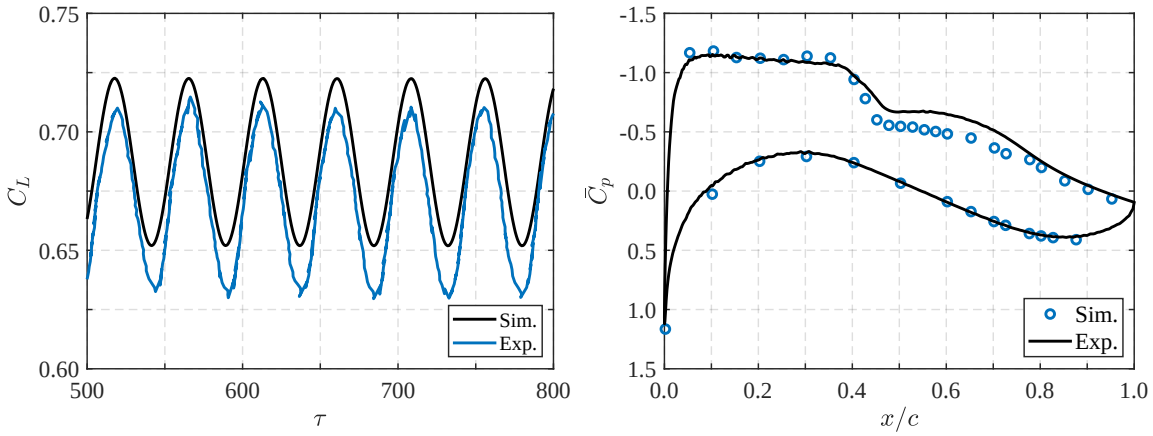

(a) Lift coefficient (b) Mean pressure coefficient

Figure 4: Comparison between computed and experimental lift coefficient time history and mean pressure coefficient of the rigid OAT15A subject to sinusoidal gust excitation.

For the aeroelastic computations, two degree-of-freedom simulations were performed with a heave mode of natural frequency $f_h = 24.7$ Hz and modal damping $\zeta_h = 0.023$, and a pitch

mode of natural frequency $f_\theta = 30.1$ Hz and modal damping $\zeta_\theta = 0.019$, as detailed by Huvelin et. al. [16]. A chord normalised centre of gravity location of $\tilde{x}_{CG} = 0.25$ was assumed, in addition to a mass ratio of $\mu = 200$. Figure 5 then shows the normalised magnitude and phase of surface pressure fluctuations. The magnitude plot of Figure 5(a) shows the computed mean shock is approximately 3% farther downstream relative to the experiment and an overestimate of the fluctuation magnitude in the post-shock region. Figure 5(b) also shows the phase reversal is marginally understated through the shock region, however, these differences likely stem from the rigid aerofoil flow calculations. Overall, the aeroelastic simulations are in fair agreement with the experiments, instilling confidence in the aeroelastic simulation framework adopted in this study.

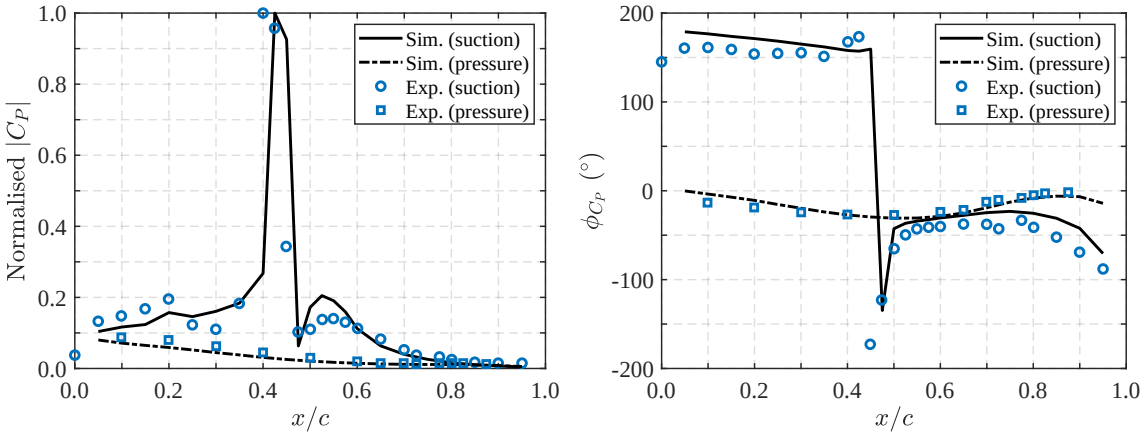

(a) Magnitude (b) Phase

Figure 5: Comparison between computed and experimental pressure magnitude and phase of the elastically-suspended OAT15A subject to sinusoidal gust excitation.

3.3 Single-degree-of-freedom pitch response

Shock buffet lock-in, or frequency synchronisation between the structural and buffeting flow, has been studied somewhat extensively in recent literature for two-dimensional pitching profiles modelled as a linear oscillator [2, 12, 22–24]. Here, the key characteristics are reiterated for the present test case. The reader is directed to Giannelis et al. [25] for a more comprehensive analysis.

Aeroelastic computations are performed for varying wind-off pitch natural frequency at the nominal buffet condition of $Re \approx 3 \times 10^6$, $M = 0.73$, and $\alpha = 3.5°$. Figure 6 then presents the resulting pitch amplitude θ and dominant pitch response frequency $\tilde{k}_{s,\theta}$ against the wind-off pitch natural frequency $\tilde{k}_\theta$, where both $\tilde{k}_{s,\theta}$ and $\tilde{k}_\theta$ are frequency variables normalised by the rigid profile buffet frequency. The aeroelastic response is broadly characterised by three regions. For pitch eigenfrequencies below the buffet (Region A), the response amplitude and frequency remain relatively constant, with moderate amplitude oscillations evolving at a coupled response frequency approximately 10% above the rigid profile flow frequency.

Beginning at $\tilde{k}_\theta \approx 1.00$, synchronisation occurs between the aerodynamic and structural modes within Region B, with the pitch response frequency tracking the wind-off pitch natural frequency throughout the so-called *lock-in* region, producing large amplitude structural limit cycle oscillations. A precipitous decrease in the pitch response amplitude is observed at the offset of lock-in into Region C. Here, the system behaves in a manner characteristic of a forced linear oscillator, with the pitch response driven at a frequency equivalent to the shock oscillation. It

should be noted that transitional behaviours exist between the regions shown in Figure 6, and once more the reader is directed to Giannelis et al. [25] for further analysis.

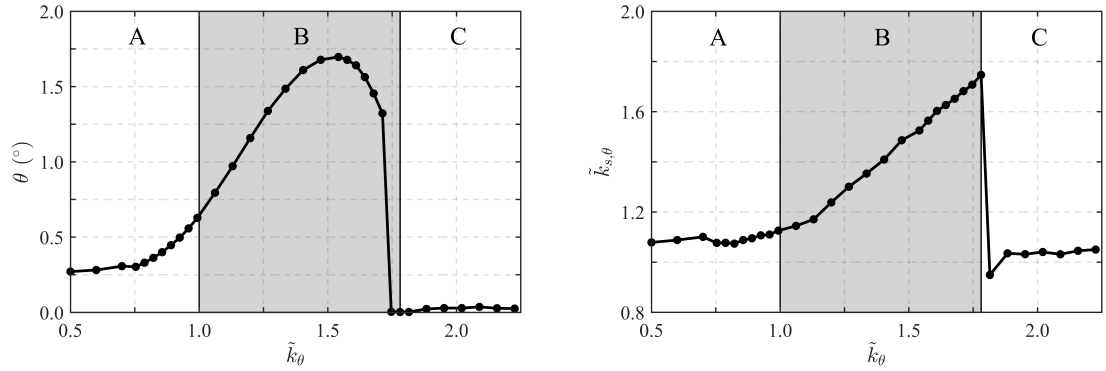

(a) Pitch amplitude (b) Dominant pitch response frequency

Figure 6: Pitch response with varying pitch natural frequency. Shading indicates lock-in region.

4 SENSITIVITY TO FREESTREAM CONDITIONS

The discussion in Section 3.1 has demonstrated a substantial sensitivity of the rigid aerofoil aerodynamic response to variations in Mach number and angle of attack. Naturally, the aeroelastic response also exhibits a degree of sensitivity to changes in freestream conditions. Studying the relationship between the structural response and flight condition is the focus of the present discussion. Simulations are performed for a single degree-of-freedom OAT15A system free to rotate in pitch. Nominal structural parameters of $\mu = 100$, $\zeta_\theta = 2\%$ and $\tilde{x}_{CG} = 0.4$ are imposed and three pitch natural frequencies are considered ($\tilde{k}_\theta = 0.7$, $\tilde{k}_\theta = 1.5$ and $\tilde{k}_\theta = 2.0$). These correspond to structural eigenfrequencies for which the aeroelastic response at the nominal buffet conditions lies within Region A, B and C, respectively. Mach number and angle of attack sweeps are then performed for each configuration to determine the bifurcation behaviour of the systems.

4.1 Mach number

To investigate the influence of Mach number on the aeroelastic response, sweeps are performed at an incidence of $\alpha = 5°$ within the range $0.65 \leq M \leq 0.75$. From Section 3.1, the rigid profile was shown to experience shock buffet at this angle of attack within $0.68 \leq M \leq 0.73$. This is indicated by the shaded region in the subsequent plots.

4.1.1 Region A

Considering first a pitch natural frequency of $\tilde{k}_\theta = 0.75$, Figure 7(a) shows the resultant bifurcation diagram of the system. Figure 7(b) also shows the two most prominent frequencies evident in the pitch response across the conditions considered, where $\tilde{f}_1$ is the dominant frequency and $\tilde{f}_2$ the secondary. Contrary to the preceding analysis, where $\tilde{k}$ denoted a reduced frequency normalised by the rigid profile buffet frequency, the parameter $\tilde{f}$ is used here to denote normalisation by the wind-off pitch natural frequency. The rigid aerofoil buffet frequency ($\tilde{f}_{sb}$) is also shown for comparison.

Figure 7(a) shows that large amplitude limit cycles develop at low Mach numbers. A smooth reduction in LCO amplitude accompanies an increase in Mach number, with the rigid profile onset boundary having no apparent influence on this relationship. At $M = 0.72$, a mild jump to a lower amplitude branch is noted. Figure 7(b) further illustrates that this point coincides

with the dominant response frequency migrating from the structural natural frequency to track the buffet frequency. This continues through to $M = 0.74$, with higher Mach numbers yielding steady solutions.

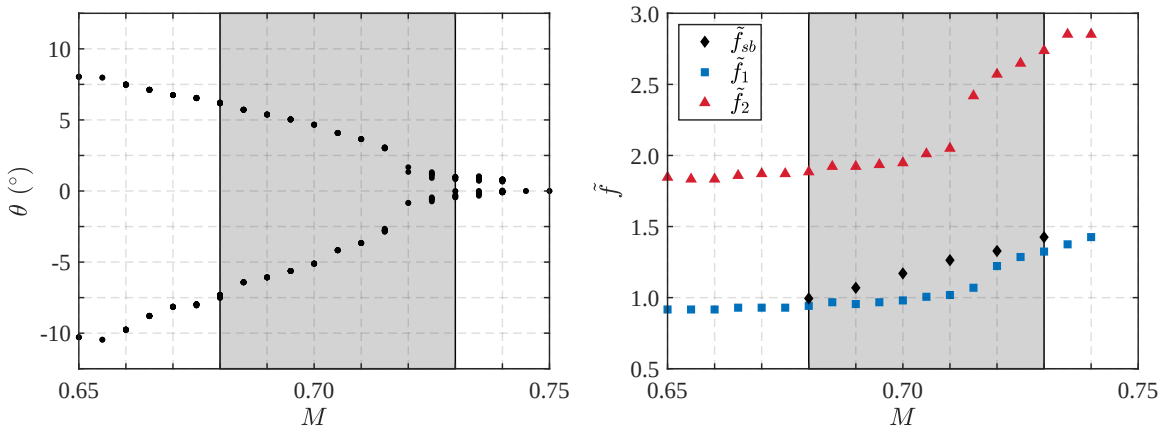

(a) Amplitude (b) Frequency

Figure 7: Amplitude and frequency bifurcation diagrams of elastically-suspended OAT15A profile with changes in Mach number ($\tilde{k}_\theta = 0.75$): Rigid profile buffet conditions .

The dominant response frequencies of Figure 7(b) indicate shock buffet synchronisation drives the aeroelastic response at low Mach numbers. For $M \leq 0.71$, the pitch response contains frequency content only at the pitch natural frequency and its harmonics. Mode switching to a coupled response primarily driven by buffet occurs at approximately $M \approx 0.72$, where the pitch response ceases to exhibit any significant spectral content at the structural frequency. This reflects a transition from a dynamic response characteristic of the lock-in Region B from Section 3.3 to a strongly coupled forced vibration akin to Region A.

The increase in LCO amplitude at conditions further removed from the buffet onset boundary appears contradictory. The behaviour here is interpreted with respect to the location of the shock oscillation region relative to the centre of gravity. At lower Mach numbers, the shock is situated farther upstream on the profile. As the shock moves upstream from the CG, an increasingly destabilising moment is imparted to the aeroelastic system, with the motion consisting of upstream shock propagation into the freestream on both the pressure and suction surfaces. This is particularly prevalent in the case of low structural eigenfrequencies, such as that of $\tilde{k}_\theta = 0.75$, where the aeroelastic system exhibits lower pitch stiffness. While this behaviour does involve shock oscillations, the instability is not driven by buffet. rather, the response here represents a more general transonic aeroelastic instability and may develop at conditions far from the buffet onset boundary.

4.1.2 Region B

Interesting dynamic behaviours emerge when considering changes in Mach number for a system of pitch natural frequency within the lock-in region ($\tilde{k}_\theta = 1.5$). Figure 8 provides the resulting bifurcation plots from Mach number sweeps at these conditions. The amplitude diagram of Figure 8(a) displays a character consistent with the nontypical LCOs of the F-16, in which a limit-cycle grows and then reduces in amplitude with an increase in Mach number, that have been observed in flight testing and detailed by Denegri [26]. Figure 8(a) shows precisely this behaviour. LCO amplitude grows and reduces marginally for $M \leq 0.68$. At this condition, where the rigid aerofoil onset boundary exists, low-amplitude oscillations develop in the pitch

response. These continue through to $M = 0.71$, where a discontinuous jump phenomenon drives the system to a large amplitude branch. These large amplitude oscillations persist up to $M = 0.74$, where the magnitude of the pitch response again begins to diminish.

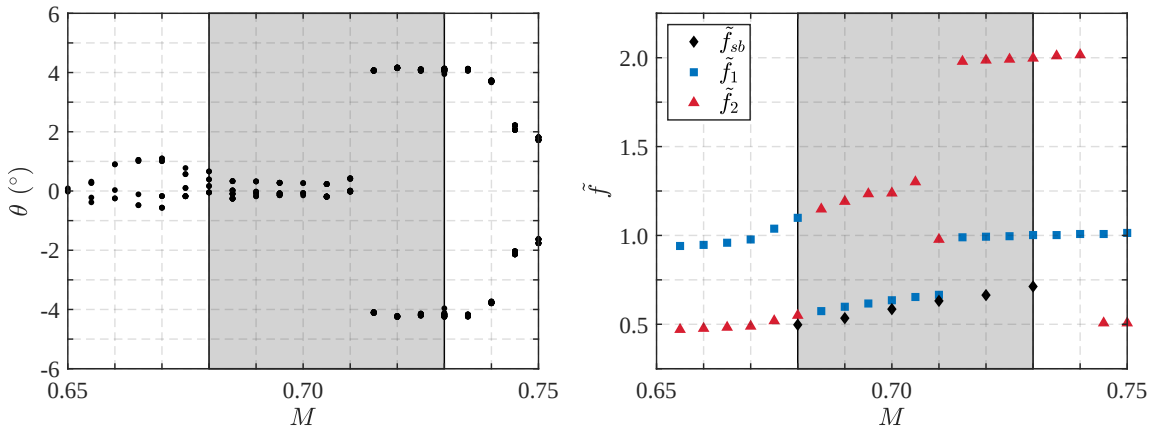

(a) Amplitude (b) Frequency

Figure 8: Amplitude and frequency bifurcation diagrams of elastically-suspended OAT15A profile with changes in Mach number ($\tilde{k}_\theta = 1.5$): Rigid profile buffet conditions .

The frequency behaviour of Figure 8(b) provides further insight on this emergence of such nontypical LCOs. The initial increase in amplitude at low Mach number develops as the pitch response oscillates at the structural mode's natural frequency. An increase in Mach number results in the response migrating from the pitch mode to the buffet mode. Within the Mach region for which rigid buffet develops, the aeroelastic response adopts a forced vibration character at a coupled frequency approximately equal to the buffet (and its harmonics). As for the $\tilde{k}_\theta = 0.75$ case, this is characteristic of Region A behaviour from the lock-in maps of Figure 6. The jump bifurcation results from an abrupt mode switching in the pitch response, as the forced vibration motion migrates to lock-in. The pitch response remains synchronised with further increases in Mach number, with the amplitude beginning to diminish as the secondary mode switches from a superharmonic to a subharmonic of the fundamental pitch mode.

The dynamic behaviour discussed above is conveniently represented through the phase portraits and wavelet spectra provided in Figure 9. The responses at low Mach numbers are highly periodic. The period-2 limit cycles that develop for $M \leq 0.68$ are entirely dictated by the wind-off structural mode, with Figure 9(d) showing frequency content at half the pitch natural frequency and its higher-order harmonics. The low-amplitude oscillations occurring for $0.68 < M \leq 0.71$ maintain a period-2 or cardioid-type phase portrait and Figure 9(e) shows the coupled pitch response exhibits frequency content at approximately the rigid buffet frequency and its harmonics. Following the jump phenomenon, the associated nontypical LCO behaviour exhibits a quasiperiodic response of spectral content primarily at the structural mode superimposed with low-frequency, intermittent and broader-band oscillations, as shown in Figure 9(f).

The key observation from the preceding analysis is the potential for nontypical LCOs to develop in the presence of transonic buffet. The root cause of this instability, particularly following its identification on the F-16 aircraft, was contentious within the research community. Both nonlinear structural mechanisms [27, 28] and flow nonlinearities [29], including shock-induced separation and general compressibility and viscous effects have been suggested. The analysis performed in this study implies a relationship to buffet synchronisation, with the nontypical

LCOs developing at Mach numbers for which lock-in occurs. A confirmation of this hypothesis would necessitate further study and is left as an avenue for future work.

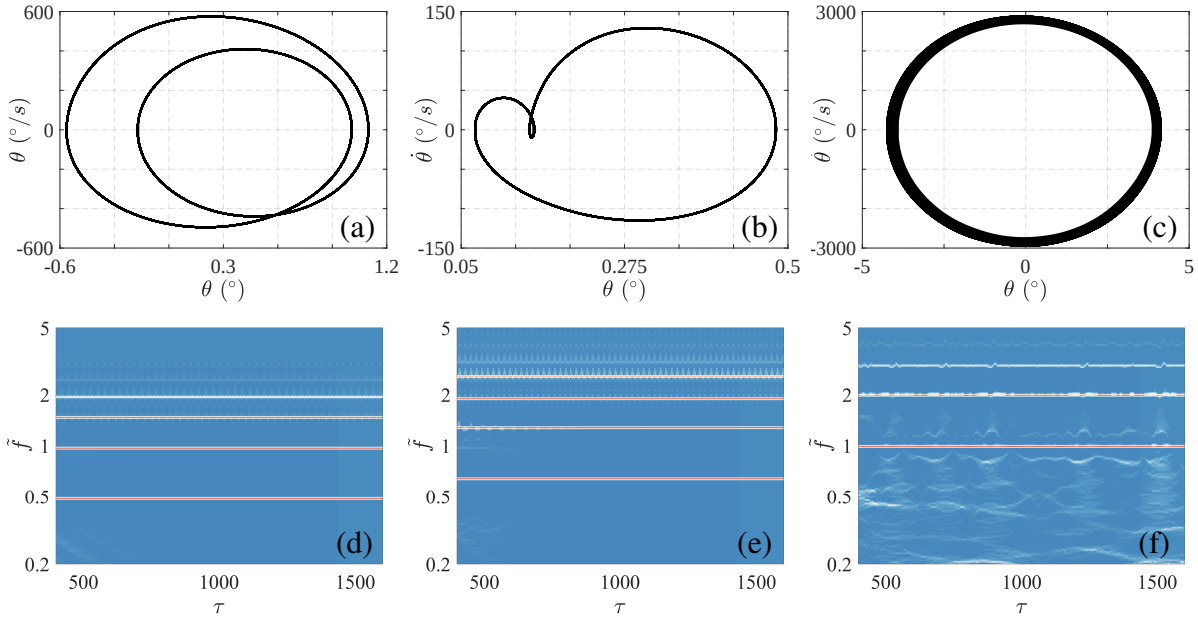

Figure 9: Phase portraits & wavelet spectra of the OAT15A pitch response at $\alpha = 5°$, $\tilde{k}_\theta = 1.5$ and: (a) & d) - $M = 0.67$; (b) & (e) - $M = 0.70$; (c) & (f) - $M = 0.73$.

4.1.3 Region C

Figure 10 provides the bifurcation plots for the combination of structural parameters corresponding to a Region C, two-frequency forced vibration response ($\tilde{k} = 2.0$). Steady responses are evident for $M \leq 0.66$. A bifurcation point exists at $M \approx 0.66$, from which increasing amplitude pitch oscillations develop.

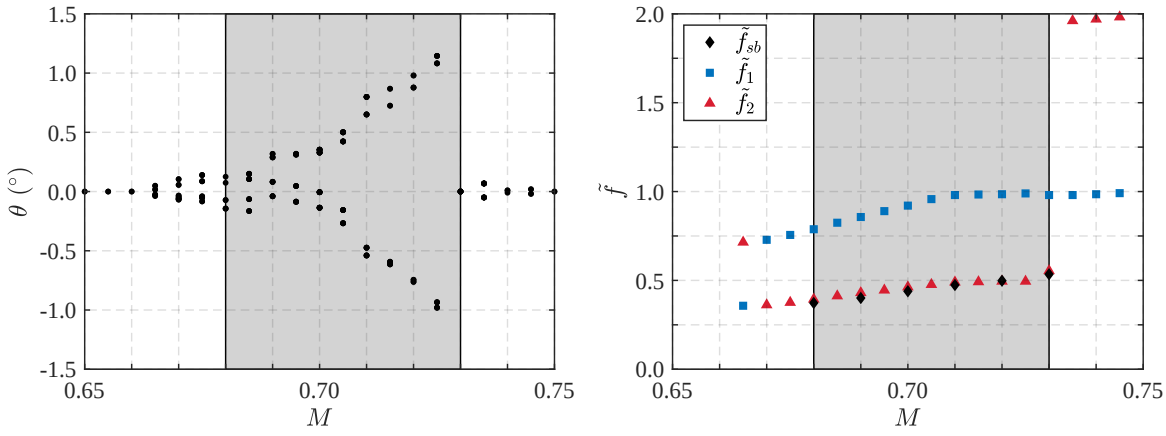

(a) Amplitude (b) Frequency

Figure 10: Amplitude and frequency bifurcation diagrams of elastically-suspended OAT15A profile with changes in Mach number ($\tilde{k}_\theta = 2.0$): Rigid profile buffet conditions .

Although this condition lies outside the rigid aerofoil buffet boundary, Figure 10 indicates the coupled pitch response approximately follows the trend of the rigid buffet frequency for Mach numbers below the onset bounds. With further increases in Mach number, the dominant frequency continues to track the buffet mode as increasing amplitude oscillations ensue.

A jump phenomenon is also evident under this configuration at $M = 0.73$, however, contrary to $\tilde{k}_\theta = 1.5$, this now relates to the transition from an LCO to steady response and occurs at the upper bounds of the rigid buffet envelope. For larger Mach numbers, the system responds purely at the structural natural frequency and its harmonics. At these conditions the buffet instability does not appear, and the structural response is similar to an SDOF oscillator subject to freestream flow excitation.

4.2 Angle of attack

To explore the sensitivity of the aeroelastic response to variations in incidence, angle of attack sweeps are conducted at the nominal Mach number $M = 0.73$ and span $2° \leq \alpha \leq 9°$.

4.2.1 Region A

The resulting bifurcation diagrams for a system of pitch natural frequency $\tilde{k}_\theta = 0.75$ are given in Figure 11. The low-incidence steady solutions develop into periodic oscillations for $\alpha \geq 2.5°$. The symmetric branching shown in Figure 11(a) and transition to bounded periodic oscillations from a steady equilibrium is characteristic of a Hopf bifurcation, analogous to that shown to incite the buffet instability in rigid systems [7, 30]. The results further indicate a reduced onset incidence for transonic systems when aeroelastic effects are taken into consideration, similar to the findings of Gao et. al. [31].

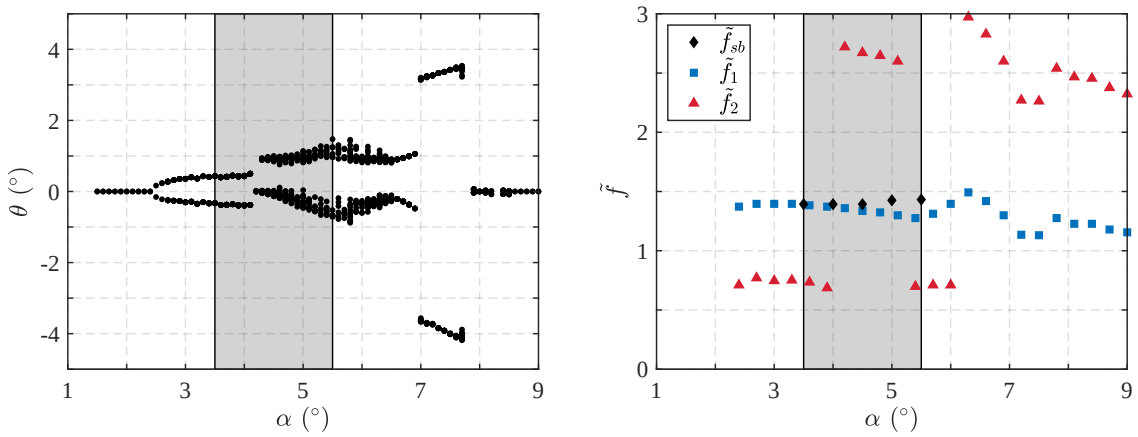

(a) Amplitude (b) Frequency

Figure 11: Amplitude and frequency bifurcation diagrams of elastically-suspended OAT15A profile with changes in angle of attack ($\tilde{k}_\theta = 0.75$): Rigid profile buffet conditions .

A secondary bifurcation point is apparent at $\alpha = 4.2°$, where the low-incidence periodic and symmetric LCOs adopt a quasiperiodic and asymmetric character. The response regains a periodic nature at $\alpha \approx 6.5°$, prior to a jump to a large amplitude branch at $\alpha \approx 7°$. This branch only exists as a stable solution for a narrow band of incidence, and the response returns to a low-amplitude limit cycle oscillating at a coupled frequency approximately equal to the buffet.

Figure 12 provides the phase plane trajectories and wavelet spectra for angles of incidence that typify the post-Hopf, quasiperiodic and large amplitude responses noted from Figure 11(a). Two interesting observations are made, particularly by considering the wavelet spectra. Figure 12(e) shows that in addition to the fundamental flow frequency and its harmonics, broadband spectral content is evident at low frequencies. This is clearly the source of the quasiperiodicity observed in Figure 12(b) and represents a broad spectral bump at frequencies incommensurate with both

the buffet and structural natural frequencies. The time-frequency response of Figure 12(f) indicates that the pitch response initially follows a frequency associated with the aerodynamic mode, prior to an abrupt transition to a coupled response of frequency between the wind-off pitch and the aerodynamic modes. These characteristics suggest a distinct mechanism driving the aeroelastic response at higher incidence.

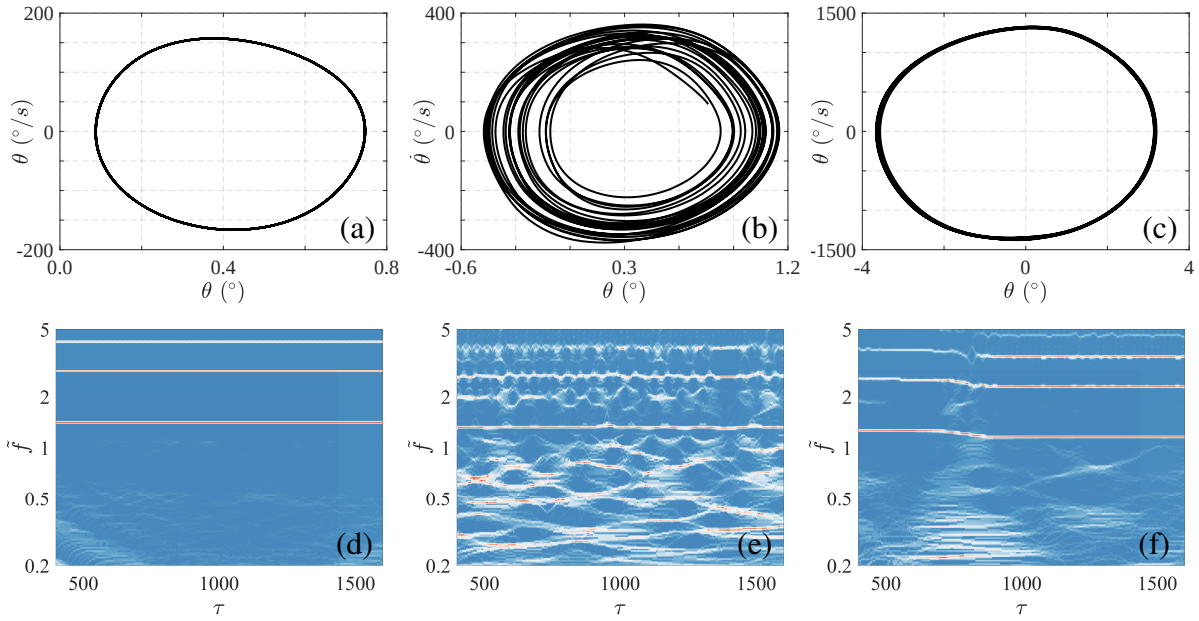

Figure 12: Phase portraits & wavelet spectra of the OAT15A pitch response at $M = 0.73$, $\tilde{k}_\theta = 0.75$ and: (a) & d) - $\alpha = 3°$; (b) & (e) - $\alpha = 5°$; (c) & (f) - $\alpha = 7°$.

The pitch response across the entire incidence range for $\tilde{k} = 0.75$ is governed by the fluid, as was found for the nominal freestream conditions. The dominant frequency plot of Figure 11(b) shows the coupled response frequency follows the buffet throughout and well beyond the rigid aerofoil buffet boundary, with the secondary frequency emerging at either subharmonics or superharmonics of the fundamental flow. Ultimately, the aeroelastic response maintains the Region A characteristics discussed in Section 3.3 regardless of the incidence. However, more complex nonlinear interactions evolve at higher angles of attack. The rigid aerofoil was found to display Type A [32] oscillations throughout the buffet envelope at this Mach number. Nonetheless, the broadening of the instability region when considering aeroelastic effects may lead to more exotic shock motions, such as those discussed by Giannelis et al. [6], developing at higher angles of attack, offering a possible explanation for the distinct LCO behaviours observed in Figure 11(a).

4.2.2 Region B

While the aeroelastic behaviour is governed by the fluid mode for all incidence at low pitch eigenfrequencies, the contrary is seen for structural natural frequencies within the lock-in region. The dominant response frequency plot of Figure 13(b) for $\tilde{k}_\theta = 1.5$ illustrates the coupled system response tracks the structural mode for all angles of attack considered. The low incidence behaviour is similar to that of $\tilde{k}_\theta = 0.75$, where a supercritical Hopf-like bifurcation initiates unsteadiness at a lower incidence than was observed in the rigid system. The pitch amplitude increases linearly throughout the rigid buffet region in a manner consistent with lock-in. The behaviour is distinct at higher incidence. A jump to a marginally higher amplitude branch occurs at $\alpha = 6°$, followed by the development of quasiperiodic responses from $\alpha \approx 8°$.

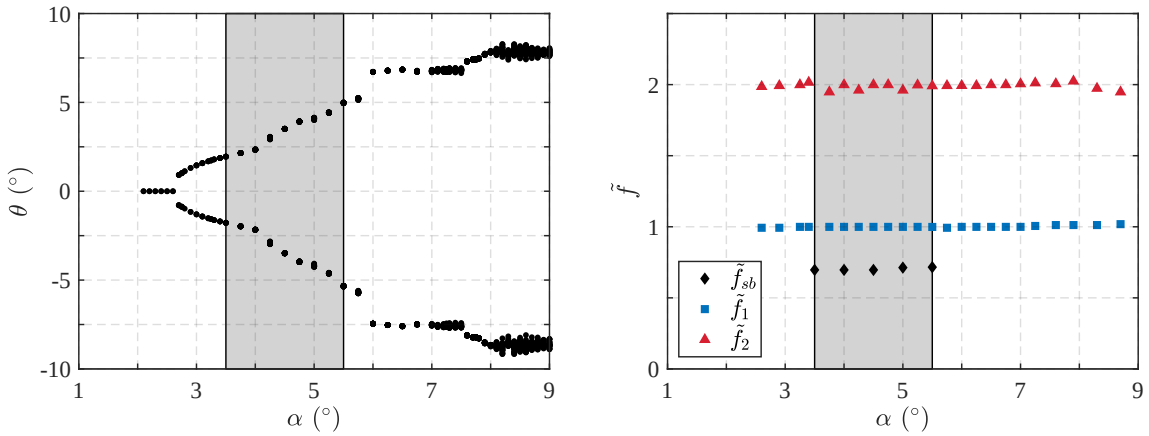

(a) Amplitude (b) Frequency

Figure 13: Amplitude and frequency bifurcation diagrams of elastically-suspended OAT15A profile with changes in angle of attack ($\tilde{k}_\theta = 1.5$): Rigid profile buffet conditions .

4.2.3 Region C

The aeroelastic behaviour across a wide range of incidence for $\tilde{k}_\theta = 2.0$ is typical of the SDOF oscillator behaviour of Region C detailed in Section 3.3. Figure 14(a) shows very low amplitude limit cycles for $\alpha \leq 7°$. The response frequency characteristics of Figure 14(b) indicate the structure oscillates at its natural frequency outside of the rigid aerofoil buffet bounds, while experiencing forced vibration at the buffet frequency within. Similar to the low pitch eigenfrequency response, a jump phenomenon occurs at $\alpha = 7°$. A smaller secondary jump emerges at $\alpha = 7.4°$, with the limit cycle amplitude continuing to grow with a further increase in incidence.

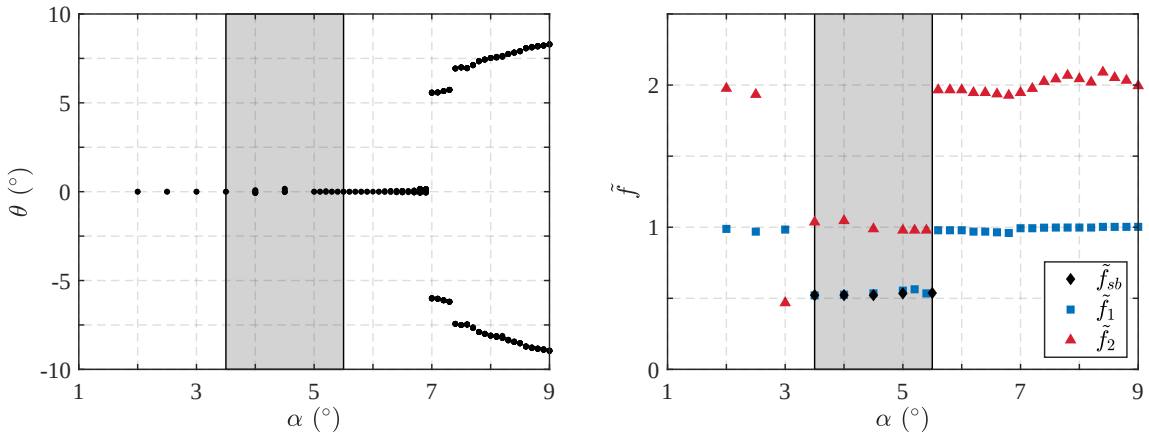

(a) Amplitude (b) Frequency

Figure 14: Amplitude and frequency bifurcation diagrams of elastically-suspended OAT15A profile with changes in angle of attack ($\tilde{k}_\theta = 2.0$): Rigid profile buffet conditions .

Considering the three characteristic structural configurations in whole, the aeroelastic response is shown to exhibit a significant sensitivity to changes in angle of attack. In particular, the switching to large amplitude branches at higher incidence indicates a fundamental shift in the governing dynamics. In the light of prior studies [1, 6], it is likely these distinct responses develop from a change in shock dynamics, particularly as aeroelastic effects broaden the instability boundaries and may yield interactions between an oscillating shock and stalled flow at high incidence.

5 CONCLUSION

This paper has undertaken a computational study on the influence of freestream conditions on the evolution of transonic limit cycle oscillations. Unsteady Reynolds-Averaged Navier-Stokes simulations have been coupled to a rigid-body structural solver and verified against available wind tunnel experimental data, demonstrating the efficacy of the applied methods. A range of coupled aeroelastic simulations have then been conducted at freestream conditions for which the rigid system experiences self-sustained shock oscillations to study the connection between transonic buffet, frequency lock-in and transonic aeroelastic limit cycle responses.

The primary findings of this work are the observed relationships between the structural response of an elastically-suspended aerofoil subject to transonic buffet conditions and the freestream flight conditions. Through basic application of bifurcation theory, a connection between shock buffet synchronisation and nontypical transonic limit cycles has been identified. For a system of pitch natural frequency above the buffet, a limit cycle emerges and disappears over a narrow band of Mach numbers that coincides with the Mach regime in which lock-in develops. With varying incidence, a reduction in the onset boundary relative to a rigid system is found, in addition to large-amplitude responses at high angles of attack. Further, changes in the pitch eigenfrequency resulted in fundamentally different bifurcation behaviours, with both sub- and supercritical Hopf-like characteristics and jump phenomena developing with changes in both Mach number and incidence.

6 REFERENCES

[1] Giannelis, N. F., Levinski, O., and Vio, G. A. (2018). Influence of mach number and angle of attack on the two-dimensional transonic buffet phenomenon. *Aerospace Science and Technology*, 78, 89–101.

[2] Raveh, D. E. and Dowell, E. H. (2014). Aeroelastic responses of elastically suspended airfoil systems in transonic buffeting flows. *AIAA Journal*, 52(5), 926–934.

[3] Jacquin, L., Molton, P., Deck, S., et al. (2009). Experimental study of shock oscillation over a transonic supercritical profile. *AIAA Journal*, 47(9), 1985–1994.

[4] ANSYS (2017). *Fluent 18.2 Theory Guide*. ANSYS Inc.

[5] Menter, F. R. (1994). Two-equation eddy-viscosity turbulence models for engineering applications. *AIAA Journal*, 32(8), 1598–1605.

[6] Giannelis, N. F., Levinski, O., and Vio, G. A. (2020). Origins of atypical shock buffet motions on a supercritical aerofoil. *Aerospace Science and Technology*, 107, 106304.

[7] Sartor, F., Mettot, C., and Sipp, D. (2014). Stability, receptivity, and sensitivity analyses of buffeting transonic flow over a profile. *AIAA Journal*, 53(7), 1980–1993.

[8] Forrester, A. I. J. and Keane, A. J. (2009). Recent advances in surrogate-based optimization. *Progress in Aerospace Sciences*, 45(1), 50–79.

[9] Vio, G. A., Dimitriadis, G., Cooper, J. E., et al. (2007). Aeroelastic system identification using transonic CFD data for a wing/store configuration. *Aerospace Science and Technology*, 11(2-3), 146–154.

[10] Raveh, D. E. (2009). Numerical study of an oscillating airfoil in transonic buffeting flows. *AIAA Journal*, 47(3), 505–515.

[11] Gao, C., Zhang, W., and Ye, Z. (2016). A new viewpoint on the mechanism of transonic single-degree-of-freedom flutter. *Aerospace Science and Technology*, 52, 144–156.

[12] Gao, C., Zhang, W., Li, X., et al. (2017). Mechanism of frequency lock-in in transonic buffeting flow. *Journal of Fluid Mechanics*, 818, 528–561.

[13] Brion, V., Lepage, A., Amosse, Y., et al. (2015). Generation of vertical gusts in a transonic wind tunnel. *Experiments in Fluids*, 56(7), 145.

[14] Lepage, A., Huvelin, F., Le Bihan, D., et al. (2016). Experimental investigation and control of gust load response in transonic flow. In *Proceedings of 3AF Greener Aviation 2016, Brussels, Belgium*.

[15] Huvelin, F., Dequand, S., Lepage, A., et al. On the validation and use of high-fidelity numerical simulations for gust response analysis. *AerospaceLab Journal ONERA (2018) 1–16*.

[16] Huvelin, F., Lepage, A., and Dequand, S. (2019). Experimental and numerical investigations of a 2d aeroelastic airfoil encountering a gust in transonic conditions. *CEAS Aeronautical Journal*, 10, 1101–1120.

[17] Golubev, V., Dreyer, B., Visbal, M., et al. (2009). High-accuracy viscous simulations of gust interaction with stationary and pitching wing sections. In *Proceedings of the 47th AIAA Aerospace Sciences Meeting, Orlando, FL*.

[18] Giannelis, N. F., Geoghegan, J. A., and Vio, G. A. (2016). Gust response of a supercritical aerofoil in the vicinity of transonic shock buffet. In *Proceedings of the 20th Australasian Fluid Mechanics Conference, Perth, Western Australia*.

[19] Singh, R. and Baeder, J. D. (1997). Direct calculation of three-dimensional indicial lift response using computational fluid dynamics. *Journal of Aircraft*, 34(4), 465–471.

[20] Parameswaran, V. and Baeder, J. D. (1997). Indicial aerodynamics in compressible flow-direct computational fluid dynamic calculations. *Journal of Aircraft*, 34(1), 131–133.

[21] Da Ronch, A. (2012). *On the calculation of dynamic derivatives using computational fluid dynamics*. Ph.D. thesis, University of Liverpool.

[22] Gao, C., Zhang, W., and Li, X. (2019). Passive feedback control of transonic buffet flow. *Physics of Fluids*, 31(4), 046103.

[23] Giannelis, N. F. and Vio, G. A. (2018). On the effect of control surface deflections on the aeroelastic response of an aerofoil at transonic buffet conditions. In *Proceedings of the 28th International Conference on Noise and Vibration Engineering, Leuven, Belgium*.

[24] Giannelis, N. F., Murray, A. J., and Vio, G. A. (2019). Application of the Hilbert-Huang Transform in the identification of frequency synchronisation in transonic aeroelastic systems. In *Proceedings of the AIAA Scitech 2019 Forum, San Diego, CA (AIAA Paper 2019-1341)*.

[25] Giannelis, N. F. and Vio, G. A. (2020). A modal approach to shock buffet lock-in analysis. In *Proceedings of the 29th International Conference on Noise and Vibration Engineering, Leuven, Belgium*.

[26] Denegri, C. M. (2000). Limit cycle oscillation flight test results of a fighter with external stores. *Journal of Aircraft*, 37(5), 761–769.

[27] Mignolet, M., Liu, D., and Chen, P. C. (1999). On the nonlinear structural damping mechanism of the wing/store limit cycle oscillation. In *Proceedings of the 40th Structures, Structural Dynamics, and Materials Conference and Exhibit, St. Louis, MO*.

[28] Chen, P. C., Sulaeman, E., Liu, D., et al. (2002). Influence of external store aerodynamics on flutter/LCO of a fighter aircraft. In *Proceedings of the 43rd AIAA/ASME/ASCE/AHS/ASC Structures, Structural Dynamics, and Materials Conference, Denver, CO*.

[29] Thomas, J., Dowell, E., Hall, K., et al. (2007). Virtual aeroelastic flight testing for the F-16 fighter with stores. In *Proceedings of the 2007 US Air Force T&E Days, Orlando, FL*.

[30] Crouch, J. D., Garbaruk, A., and Magidov, D. (2007). Predicting the onset of flow unsteadiness based on global instability. *Journal of Computational Physics*, 224(2), 924–940.

[31] Gao, C., Zhang, W., and Ye, Z. (2018). Reduction of transonic buffet onset for a wing with activated elasticity. *Aerospace Science and Technology*, 77, 670–676.

[32] Tijdeman, H. (1977). *Investigations of the transonic flow around oscillating airfoils*. PhD Thesis, TU Delft, Delft University of Technology.

COPYRIGHT STATEMENT